Med Biol Eng Comput (2013) 51:353–365
DOI 10.1007/s11517-012-1004-7

ORIGINAL ARTICLE

Experimentally validated three-dimensional finite element model of the rat for mild traumatic brain injury

Michael Lamy · Daniel Baumgartner · Narayan Yoganandan · Brian D. Stemper · Rémy Willinger

Received: 25 October 2011 / Accepted: 17 November 2012 / Published online: 29 November 2012

Abstract The aim of our work was to expand on the knowledge concerning mild Traumatic Brain Injuries (TBI), by combining numerical modeling and animal experiments within a joint approach. A three-dimensional finite element model of the rat brain and braincase was developed, and experimental acceleration pulses were applied. Pulse data were obtained from tests conducted using anesthetized rats, subjected to coronal plane rotational acceleration loadings of varying amplitudes and durations, aimed to generate mild TBI. Times of loss of consciousness were obtained. Biomechanical response parameters generally associated with TBI (stresses and strains) in the three anatomical regions, i.e., hypothalamus, thalamus and parietal cortex were analyzed. While the parameters correlated well with changes in injury severity linked to peak rotational acceleration, they were relatively insensitive to the pulse duration or times of loss of consciousness. As a consequence, new stress-time and strain-time metrics were computed, and these metrics were more efficient in predicting changes in injury severity associated both with acceleration characteristics and loss of consciousness outcomes in all three anatomical regions controlling the aforementioned behavior. Results of our analysis tend to show that time-related metrics may be more suited for the explanation of mild TBI than commonly used peak metrics in the three anatomical regions of the brain.

M. Lamy · D. Baumgartner (✉) · R. Willinger
Department of Fluid and Solid Mechanics, University of Strasbourg, IMFS, 2 rue Boussingault, 67000 Strasbourg, France
e-mail: daniel.baumgartner@unistra.fr

N. Yoganandan · B. D. Stemper
Department of Neurosurgery, Medical College of Wisconsin, Milwaukee, WI 53226, USA

Keywords Biomechanics · Finite element model · Stress–strain analysis · Traumatic brain injuries

1 Introduction

Traumatic brain injuries (TBI) represents a major health issue in our societies. Their consequences extend from temporary impairments, in cases considered to be mild, to lifelong disabilities or death for the most severe cases. In Europe, it has been estimated that among a population of 100,000 persons, 235 would sustain TBI occurrences [41]. In the United States, according to the 2010 report issued by the Centers for Disease Control and Prevention, about 1.7 million occurrences of TBI are reported annually, among which 52,000 would end in the death of the victim of TBI, and 275,000 would result in hospitalizations [9]. Falls are the first cause of TBI, followed by motor-vehicle collisions (which becomes the first cause in terms of mortality rate) and sports-related activities. Very young children (0–4 years), adolescents and young adults (16–24 years) and adults aged 65 years or older are most likely to be the affected groups of the population, according to the report. Moreover, the impact of TBI on the economics of a country should not be neglected: not only do they cost directly in terms of health treatments, but also have a long-term financial impact, as victims of TBI-induced severe disabilities might no longer be able to be productive. Thus, over the past years, protective systems in automotive environments and protective equipment in sports have been developed and continually improved to reduce the severe outcomes and mortality rate of TBI.

Improved understanding of the biomechanics of head injuries is critical to achieve better protection. Mechanisms of TBI have been postulated to be correlated to the

complex loading conditions of collision forces, with a major focus on head acceleration [14]. Two components of this mechanical parameter can be distinguished in real life collisions: linear and rotational parts, both with direct consequences for injuries. Linear accelerations have been depicted to be generally the cause of focal brain injuries and have been correlated to intracranial pressure changes [25]. The Head Injury Criterion, HIC, based on the linear acceleration of the head, is a widely used index for designing automotive protective structures, albeit it has generated some controversies over the years [44]. Indeed, the other component of acceleration, the angular part, has also long been established as an important parameter in brain injury mechanisms [17]. It has even been reported to be responsible for the main contribution to TBI compared to linear acceleration [13, 46]. Nevertheless, it is rarely taken into account for the validation of protective systems [19].

In any case, studies have often focused on moderate to severe cases of TBI, graded as Abbreviated Injury Score, AIS 4–6 [1]. Fewer studies have been dedicated to mild TBI, in spite of the fact that these injuries can be responsible for lifelong disabilities. Ongoing military and its related involvements for approximately 10 years around the world have brought this issue more to the forefront [26, 27, 32]. Being able to predict and prevent mild TBI is important because treatments continue to be primarily based on clinical assessments without clear evidence of detectable lesions, but still have a lasting impact on the daily life of the TBI victim [15, 43]. Rat models have been widely used in neurotrauma studies and have documented physiological and behavioral deficits from different types of insults: controlled cortical impact [8, 23], dynamic cortical deformation (DCD) [39], fluid percussion [7, 24], direct head impact weight-drop [33] and rotational accelerations [5, 10, 11]. As a majority of studies have focused on severe level brain traumas such as diffuse axonal injuries (DAI), a need exists for the development of mild TBI models using rotational acceleration as the mechanical insult. Outcomes from mild TBI-specific experiments can be used to exercise finite element models to determine the local responses of the rat brain. The following table summarizing a brief review of rat finite element models is intended to demonstrate gaps in our knowledge and serve as a basis for the present computational study, aimed to determine the intrinsic responses of different anatomical regions of the brain.

Based on the foregoing observations and brief review, summarized in Table 1, and the importance of region-specific responses, a finite element model of the rat head was developed to better understand the biomechanical behavior under mild TBI conditions. Specifically, mechanical variables were extracted in regions susceptible to alterations following mild TBI induced by rotational accelerations of varying magnitudes and pulse durations.

2 Methods

2.1 Finite element model development

Medical imaging techniques were used to obtain the three-dimensional model of the head of a male Sprague-Dawley rat. The rat under study was 8–9 weeks old and weighted 350 g. Rat skull geometry was obtained from micro-computed tomography images with voxel size: 93 μm × 93 μm × 93 μm. The soft tissue geometry was extracted from magnetic resonance images with voxel size 500 μm × 500 μm × 500 μm. The extraction of geometrical data was realized by thresholding the medical images, and provided a surface triangular mesh of the brain external surface. This surface served to delimit the volume to be meshed to represent the brain in the finite element model. The meshing exercise was performed using commercial software (Altair HyperMesh 10.0©, Troy MI, USA) to define the volume which was to become the brain mesh. Elements in the models were exclusively eight-node hexahedral elements and four-node shell elements with a standard Lagrange integration scheme. The minimum edge-size for the elements was chosen as 0.45 mm; the average edge-size is consequently of 0.5 mm. Other criteria were defined and strictly monitored so that the resulting mesh would be as regular as possible. The chosen values were based on those used for the Strasbourg University Finite Element Head Model (SUFEHM) [6]. The maximum warpage was fixed at 40°, the maximum aspect ratio was defined as equaling 5, and the cut-off value for skewness was chosen at 60°. Meanwhile, the minimum jacobian was 0.7. The whole mesh was achieved with these cut-off values, and elements were manually improved one by one when they would not verify one of those values.

A first complete mesh was achieved with those criteria, with a total of 17,972 hexahedral elements and 3,220 shell elements. Then, a refined mesh was created by splitting the elements of this first mesh: one hexahedral element would be divided into eight smaller ones, while one shell element would result in four smaller ones. The new refined mesh that was obtained resulted in a minimal edge-size of 0.2 mm, which an average edge-size situated around 0.25 mm. Other criteria for the mesh were still well respected by the split mesh. The maximal reported warpage is 27.54°. The maximum aspect ratio was observed as 3.49, with less than 1 % of the elements having an aspect ratio higher than 2.5. Less than 0.2 % elements have a skewness higher than 60°, with the maximal value being 63.43°; overall, 90 % of the elements have a skewness lower than

Table 1 Computer models in literature

Model (year)	Short description	Type of simulation
Shreiber [38]	3D model made of hexahedral elements. Homogeneous, isotropic, modified hyperelastic material law for the brain; gray matter only	Dynamic cortical deformation (DCD) experiments: nine different pulses (three pressure levels, three durations). Suggests that blood–brain barrier damage is most sensitive to maximal principal logarithmic strain
Gefen [12]	Three idealized 2D cross-sectional models. Linear viscous elastic material law for the brain	The model was used to characterize the material properties of the braincase by simulating indentation experiments
Pena [36]	2D model. Homogeneous, isotropic linear elastic brain. Three cases were studied for the Young modulus E: constant (50 kPa), linear ([10; 100] kPa) or inverse linear ([100; 10] kPa)	Controlled cortical impacts (CCI) were simulated. Displacements were observed, as well as mean stresses and shear stresses. The linear variation of E was reported as showing the most likely stress distribution
Levchakov [22]	3D model made of tetrahedral elements. Homogeneous, isotropic, viscous elastic brain; gray matter only	Simulation of closed head impact injury. Brain displacements were studied. The aim was to observe the influence of age on mechanical responses such as stresses and strains
Mao [28]	3D high definition model made of hexahedral elements. Homogeneous, isotropic, viscous elastic brain. Gray and white matters were differentiated. Brain anatomical components are present	Validated against DCD data, it was used to simulate different CCI cases. Simulations indicated first principal strain as a significant parameter that best correlated with experimentally observed injuries
Fijalkowski [11]	2D model of a mid-brain coronal section. Anatomical structures were represented. The brain was depicted linear viscous elastic, with differentiated gray and white matters	Validated under three rotational loading conditions. Then, nine cases of rotational loadings, deemed responsible of mild TBI, were simulated. Sustained Maximum Principal Strain criterion was proposed correlating with experimental outcomes
Zhu [47]	Based on Mao [28] with an even more refined mesh (more than 500,000 elements)	Used to simulate blast cases under a shock tube environment. Validated against experimental pressure–time histories at the cortex and lateral ventricle. Pressure amplification was found in the skull. Low shear stress and principal strain were implied not to be injury mechanisms for blast

40°. Finally, 1 % of the elements have a Jacobian value lower than 0.7, the minimal value being 0.5; less than 0.2 % of the elements have a Jacobian lower than 0.6.

Eventually, the complete finite element mesh consisted of three main parts, which are continuous in and between themselves. The first one is the brain, composed of 118,016 hexahedral elements, and subdivided into 22 anatomical components among which 18 are internal to the cerebrum. The brain mesh used in the present study is shown in Fig. 1, with a detailed example of a coronal section in Fig. 2. The second part of the model is a single continuous layer of 25,760 hexahedral elements, encasing the brain, which are representing the cerebrospinal fluid and the meninges as a whole. This continuous layer was chosen over shell layers of meninges in order to maintain continuity in the mesh, and also in the relative movement between brain and skull. The third and last part is the skull itself, made of 25,760 shell elements (constant thickness of 0.1 mm), which are present on the external surface of the model.

The next step in the development of the finite element model consisted of assigning material properties to the various components, performed using commercial software (Altair Hypercrash 10.0©, Troy, MI, USA). All the elements of the model were considered to be homogeneous and isotropic and all brain elements were assumed to be made of gray matter. Soft tissue mechanical behaviors were obtained from the literature: the skull and brain/skull interface were attributed properties based upon finite element modeling studies from our group and research from Wayne State University [4, 28]. Skull in particular was assigned an elastic modulus similar to the one used in the SUFEHM: though studies have shown that this elastic modulus could have lower values [16, 30], the 15 GPa was kept as the model in this work would not be used to

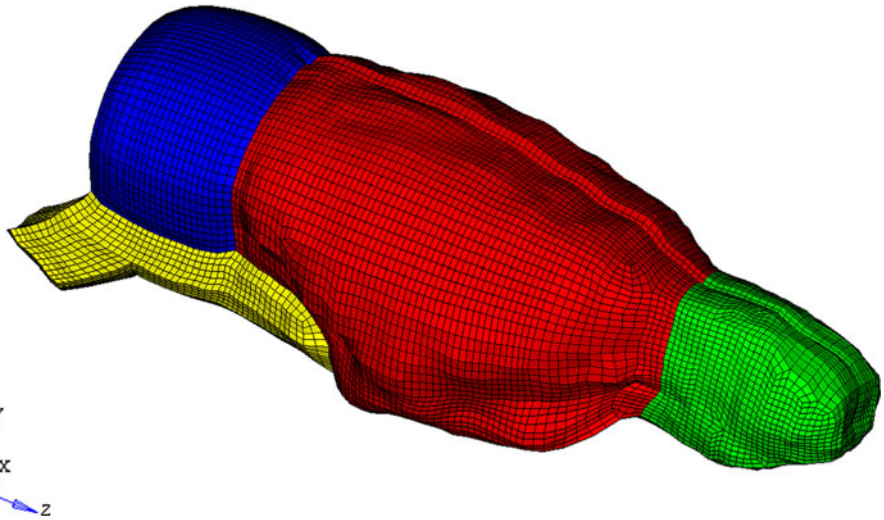

Fig. 1 Three-dimensional finite element model of the rodent brain used in the study. Proceeding from the right of the photograph are the olfactory bulbs, cerebrum, brainstem (*lower part*) and cerebellum

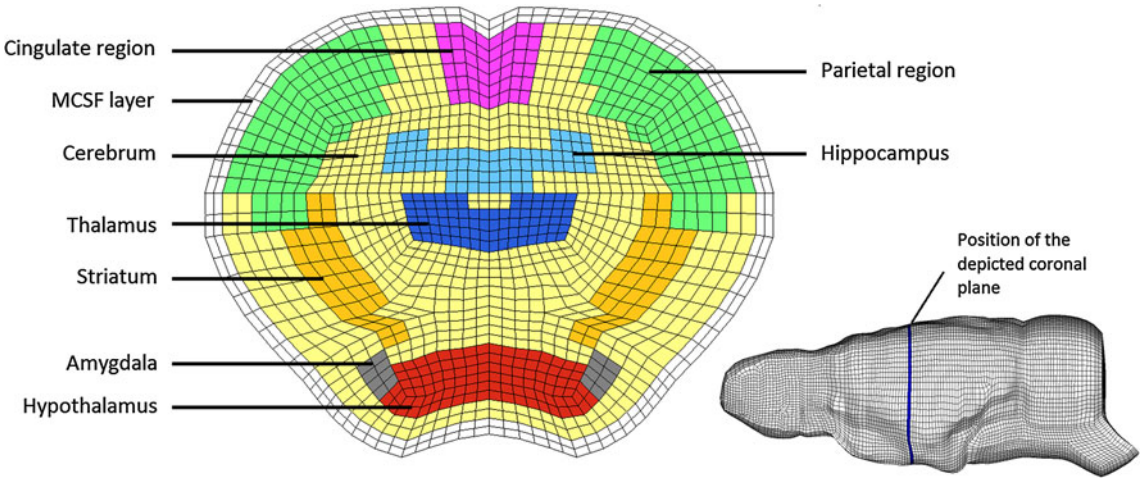

Fig. 2 A coronal section of the model (approximately Bregma—2.5 mm), with the detail of visible components. The lateral view of the model on the *right* part of the figure positions the coronal section in the model. Table 2 includes the various components simulated in the model

simulate fracture occurrences. Furthermore, the skull was defined as a rigid body for the simulations, limiting the skull elastic modulus influence. The other components representing the brain were assigned a linear viscous elastic material behavior. The Boltzman law was chosen for this purpose [12, 28]. The associated mechanical parameters were based on the literature [11]. While other material models, such as hyperelastic or nonlinear viscous elastic models, could have been chosen, there is even less available data for them than for linear viscous elastic models, even more so concerning rats. Table 2 includes the material properties in addition to the descriptions of the components used in the finite element model.

2.2 Model validation

To determine the efficiency of the model, protocols of DCD were simulated, based upon experimental data [38]. Shell elements from the skull component, as well as hexahedral elements from the layer between the skull and the brain (i.e., CSF and meninges elements), were removed to represent a craniectomy over the left cortex. Since there is only a single continuous layer of elements for both the CSF and meninges, cerebrum was directly exposed, though in the experimental setup the pia was preserved. Also, because of the geometry of the mesh, the craniectomy is squared. This shape was chosen in order to avoid redefining the mesh around the opening, which would trample with the chosen mesh criteria. Also, as the mesh would not be changed, a squared area was preferred to a rounded one to avoid unwanted additional edge effects.

The general protocol consisted in applying a vacuum pressure pulse directly on the brain elements that were exposed by the craniectomy, while the skull was granted no degree of liberty. The simulated displacements of the exposed brain surface were measured and compared to

Table 2 Material properties of the anatomical components of the model

Cerebrum (50,992), cerebellum (21,072), brainstem (11,872), olfactory bulbs (11,120), orbitofrontal cortex (3,360), cingulate cortex (1,728), parietal cortex (3,952), striatum (2,928), septum (240), thalamus (1,584), hypothalamus (1,216), amygdala (192), hippocampus (2,832), temporal cortex (592), ventral tegmental nuclei (112), mesencephalic tegmentum (256), occipital cortex (2,032), superior colliculous (752), entorhinal cortex (432), aqueduct (192), subiculum (368), inferior colliculous (192)	Density (kg/m^3)	1,040
	Short-term shear modulus (kPa)	10
	Long-term shear modulus (kPa)	2
	Bulk modulus (GPa)	2.19
	Decay constant (s^{-1})	0.125
Layer of hexahedral elements connecting the skull to the brain (single continuous layer representing the meninges and cerebrospinal fluid—25,760)	Density (kg/m^3)	1,130
	Young modulus (MPa)	20
	Poisson's ratio	0.45
Skull (25,760)	Density (kg/m^3)	1,800
	Young modulus (MPa)	15,000
	Poisson's ratio	0.21

Numbers of elements are indicated in parentheses

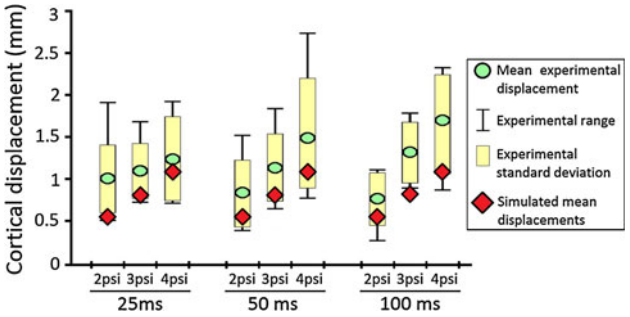

Fig. 3 Experimental and simulated cortical displacements (experimental data are reported from [38])

experimental measures. This protocol was exercised in nine different simulations, representing all the combinations of pressure pulse amplitude (25, 50 and 100 psi) and duration (25, 50 and 100 ms) from the experimental set.

Results are displayed on Fig. 3. Reported simulated displacements are the mean value for the nine nodes situated in the region of maximal observed deformation. This region and the nine selected nodes were consistent for all nine simulations.

Simulated displacements were of the same magnitude order than the experimental ones. They were close to the lowest experimentally measured deformation for all nine cases, and about 1.5 time lower than the experimental mean results. For a given duration, maximal displacement increased with the amplitude of the pressure pulse. On the opposite, and in accordance with experimental findings, duration of the pressure pulse had no significant effect for a given pressure amplitude.

Concerning the difference between the mean experimental displacements, and their simulated equivalents which were 1.5 time lower, the question of the material properties can be addressed. It is known that the value of some of these properties, mainly the short-term shear modulus, can affect the values of the mechanical responses of a brain model. Indeed, an increase in shear moduli would result from an increase in the frequency of the loadings [40, 42]. Since dynamic cortical displacements occur during 25–100 ms, they represent loadings of a lower frequency than the rotational acceleration loadings we applied for our simulations, as said accelerations happen in 1–3 ms. This suggests that a lower short-term shear modulus might be more appropriate for dynamic cortical displacements simulations, and this could be a reason for the slightly lower simulated displacements. However, the short-term shear modulus was chosen to be appropriated for the mTBI-inducing rotational accelerations protocols [11]. As a matter of fact, the choice of the DCD protocol for validation purpose could be argued since this protocol is extremely different from the angular acceleration one. However, and because of the paucity of available data, which can be used for validation investigation, the DCD protocol was still chosen.

2.3 Numerical simulations

The finite element model was exercised under different coronal plane rotational acceleration pulses. As skull fractures were not planned in these simulations, the skull was treated as a rigid body. Hence, rotational accelerations were applied directly to the skull. Each loading case, representing a specific pulse, was based upon experimental angular acceleration versus time data [11]. Figure 4 shows a representative plot of the rotational acceleration versus time history. The rotational accelerations and time durations are included in Table 3. While each numerical simulation received the loading conditions of its respective experimental group (described later), they all shared the same material properties. The stress analysis was conducted using commercial software (Radioss Crash© solver, Altair HyperMesh 10.0©, Troy, MI, USA), on a standard

personal computer with an Intel core 2 DUO© processor running at 3.33 GHz with 2 GB of RAM. In terms of performances, simulations were conducted for 10 ms durations and generally took nearly an hour of computational calculation time to be completed. The hourglass energy of the model was nullified using a HEPH 8-node linear element with reduced integration point and physical stabilization of hourglass.

Mechanical responses at tissue levels were obtained from the numerical simulations. The stress analysis output was extracted for the following three anatomical regions in the brain; hypothalamus, thalamus and parietal cortex. Reasons for using these regions are discussed later. Strain and stress data were used to compare responses in these regions to the loss of consciousness times obtained from experiments [11]. Specifically, maximum principal strains and Von Mises stresses were evaluated. For each parameter, anatomical distributions were analyzed; at the same time, time history data was obtained for each element in the model, and then the mean values of the parameter for every anatomical region were evaluated as functions of time. In the end, anatomical distributions and peak mean values of the studied parameters were used to determine the consequences of the rotational acceleration loading. Results are presented in two groups: increasing rotational accelerations with constant time durations and increasing time durations with constant rotational accelerations. Data are illustrated for the hypothalamus, followed by the thalamus and parietal cortex regions.

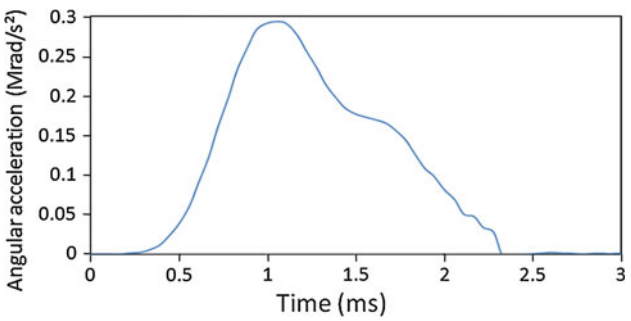

Fig. 4 Representative acceleration-time history inputted to the finite element model

3 Results

Table 3 lists the whole set of acceleration pulses. The central case has a maximum rotational acceleration of 419 krad/s^2 for 2 ms duration. Pulses are ordered in two groups. Group A pulses have similar durations (2 ms) with increasing rotational accelerations (from 292 to 523 krad/s^2) while group B pulses have similar rotational accelerations (425 krad/s^2) with increasing durations (from 1 to 3 ms). The central case (419 krad/s^2 for 2 ms) is shared between the two groups as the medium pulse for both of them. All cases were based on six samples, except the medium case, which had seven.

Table 3 also reports the observed average durations during which the rats of the different groups remained unconscious. Those are the unconscious times attributed to the effects of the acceleration pulses only. A sham group of uninjured rats had been observed to need 120 s to recover from the anesthesia. Unconscious times in Table 3 correspond to the additional durations needed by the rats to recover after these 120 first seconds. Increasing amplitudes (with fixed duration) or increasing duration (with fixed amplitude) of the loading pulse both resulted in increasing unconscious times.

3.1 Strains: hypothalamus, parietal cortex and thalamus

The maximum principal strain responses in the hypothalamus, parietal cortex and thalamus for the two groups of pulses are displayed in Fig. 5. For each of the three regions, strains increased with increasing amplitude of the loading pulse (while its duration was fixed). In contrast, a similar trend was not apparent when the amplitude was fixed and duration was increased.

3.2 Strain rates: hypothalamus, parietal cortex and thalamus

Strain rates in the three regions presented the same observations as strains, i.e., increasing rates with increasing amplitude of acceleration (fixed duration), but no apparent trend when amplitude was fixed and duration increased. These data are shown in Fig. 6.

Table 3 Pulses for the two groups along with experimentally determined unconscious times

Nomenclature	Units	Group A			Group B		
		Low	Medium	High	Low	Medium	High
Average values ± standard deviation							
Rotational acceleration	krad/s^2	292 ± 34	419 ± 29	523 ± 15	424 ± 24	419 ± 29	427 ± 21
Duration	ms	2.1 ± 0.2	2.0 ± 0.2	2.0 ± 0.2	1.1 ± 0.2	2.0 ± 0.2	3.0 ± 0.1
Unconscious time	s	86 ± 44	246 ± 25	325 ± 28	80 ± 12	246 ± 24	510 ± 105

The medium case (*highlighted column*) is one and the same, but is presented twice for comparison purpose

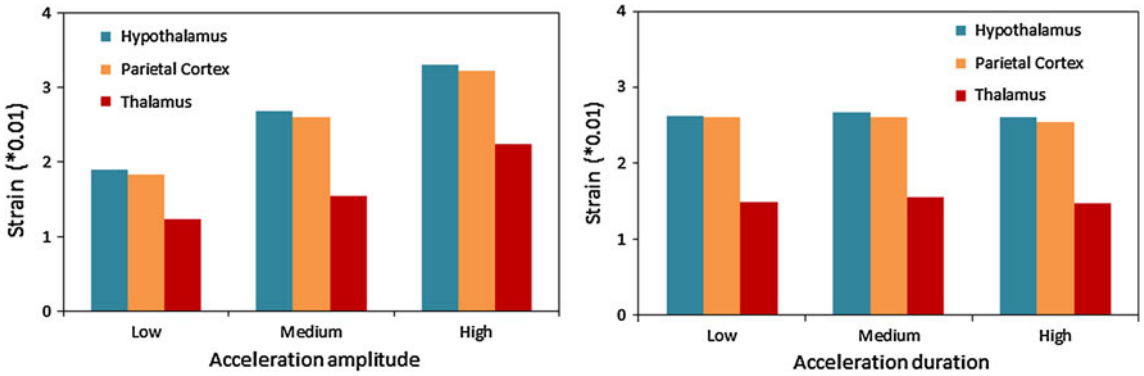

Fig. 5 Bar chart showing maximum strains in the hypothalamus, parietal cortex and thalamus. *Left* shows variations with increasing magnitude of applied rotational acceleration (fixed duration), and *right* shows variations with increasing magnitude of duration (fixed rotational acceleration)

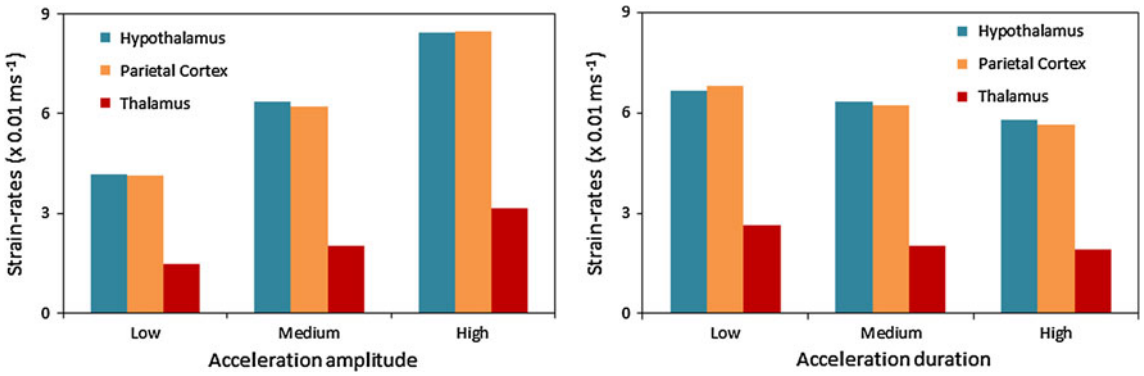

Fig. 6 Bar chart showing maximum strain rates in the hypothalamus, parietal cortex and thalamus. *Left* shows variations with increasing magnitude of applied rotational acceleration (fixed duration), and *right* shows variations with increasing magnitude of duration (fixed rotational acceleration)

3.3 Stress metrics: hypothalamus, parietal cortex and thalamus

Von Mises stress responses were similar to strain outputs in all the three anatomical regions, i.e., stresses increased with increasing amplitude of the loading pulse (fixed duration). However, a similar trend was not apparent with increasing durations when the amplitude was fixed. These are shown in the form of combined bar charts for the two groups of pulses in Fig. 7.

3.4 New metrics: the stress-time and strain-time values

Because the trends were not consistent between the two groups for all the former metrics (strains, strain-rates and stresses), a different metric was examined. It was accomplished through the use of a stress-time parameter, rationale described later. The mean Von Mises stress data history was integrated in three anatomical regions separately. Then the stress-time value was defined as the integral for the duration of the pulse. Figure 8 reports the Von Mises and integrated Von Mises stresses data histories for a typical middle duration acceleration pulse. Figure 9 demonstrates the variation of this metric for the two groups, showing improved consistency with regard to changes in magnitudes and durations of rotational acceleration pulses and between unconscious times.

In the same way, strain-times values were defined from the integrated strain data histories in the three anatomical regions. They were defined as the values of the integral for the duration of the acceleration pulse. Figure 10 depicts the strain and integrated strain data histories for a typical middle duration acceleration pulse, while Fig. 11 displays the variations of this strain-time metric, which is more consistent with variations in amplitude or duration of the rotational acceleration pulse.

3.5 Correlations of stresses and strains with unconscious times

Table 4 shows the results of a linear correlation between the unconscious times for the two groups of pulses and the stress and strain metrics for the three anatomical regions. For these correlation studies, the intercept value was forced

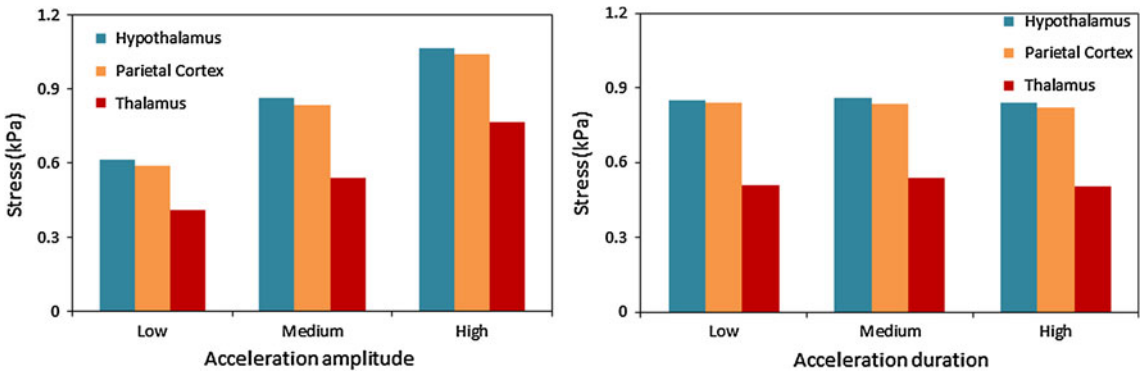

Fig. 7 Bar chart showing stresses in the different regions of the brain. *Left* shows variations with increasing magnitude of applied rotational acceleration (fixed duration), and *right* shows variations with increasing magnitude of duration (fixed rotational acceleration)

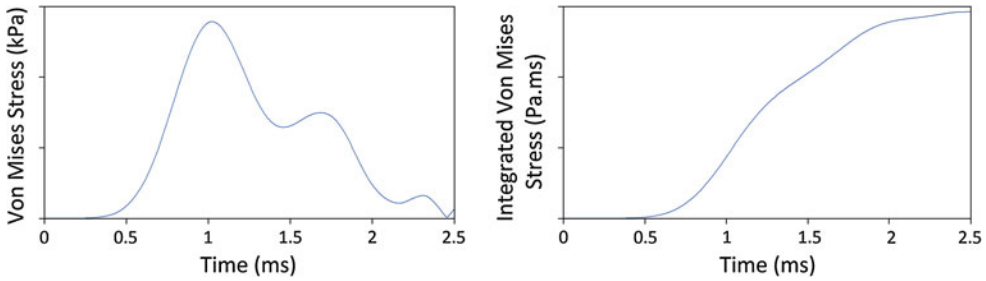

Fig. 8 Typical shapes of Von Mises stress (*left*) and integrated Von Mises stress (*right*) data histories for a middle duration (2 ms) rotational acceleration pulse. In such a case, the stress-time indicator would be the value of the integrated Von Mises stress at 2 ms time

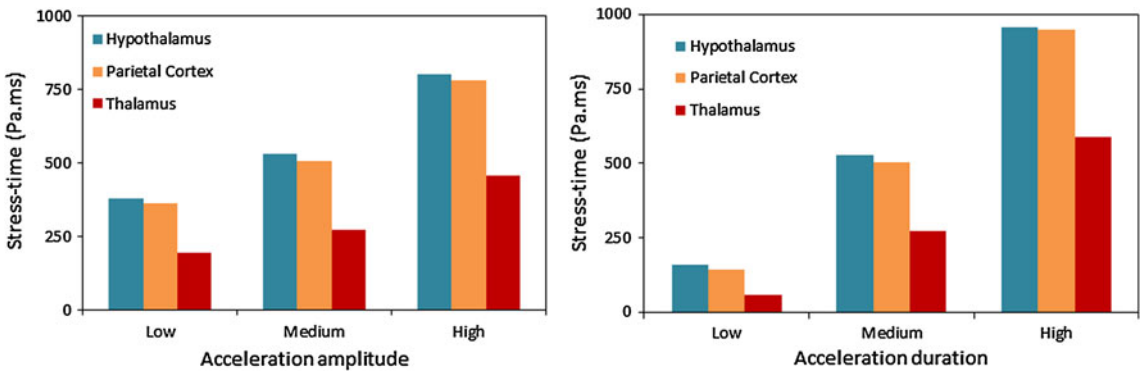

Fig. 9 Bar chart showing stress-time responses in the different regions of the brain. *Left* shows variations with increasing magnitude of applied rotational acceleration (fixed duration), and *right* shows variations with increasing magnitude of duration (fixed acceleration). Note similar trends in both groups (*left* and *right*)

to zero, since we assumed that the absence of mechanical solicitation would not cause an unconscious time (that is to say would not delay return to consciousness past the 120 s due to recovery from anesthesia). As can be seen, both the strain and stress parameters showed poor correlations while the time-related metrics responded with improved correlations, regardless of the anatomical region. However, the correlation was the greatest for the thalamus, followed by the parietal cortex and hypothalamus.

Data points and their associated regression trends are illustrated on Fig. 12 for the hypothalamus. Trends for the parietal cortex and the thalamus were mainly similar to those for the hypothalamus.

4 Discussion

4.1 On the choice of the animal model

The current three-dimensional modeling effort was undertaken to examine the region-specific intrinsic variables because data on unconscious times were available in a

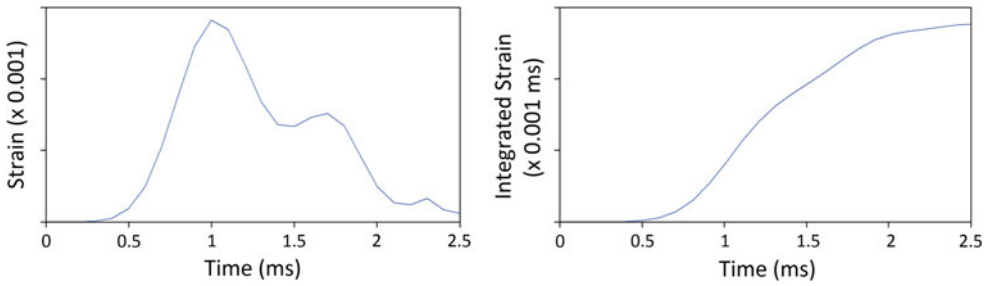

Fig. 10 Typical shapes of Maximum Principal Strain (*left*) and integrated Maximum Principal Strain (*right*) data histories for a middle duration (2 ms) rotational acceleration pulse. In such a case, the strain-time indicator would be the value of the integrated Maximum Principal Strain at 2 ms time

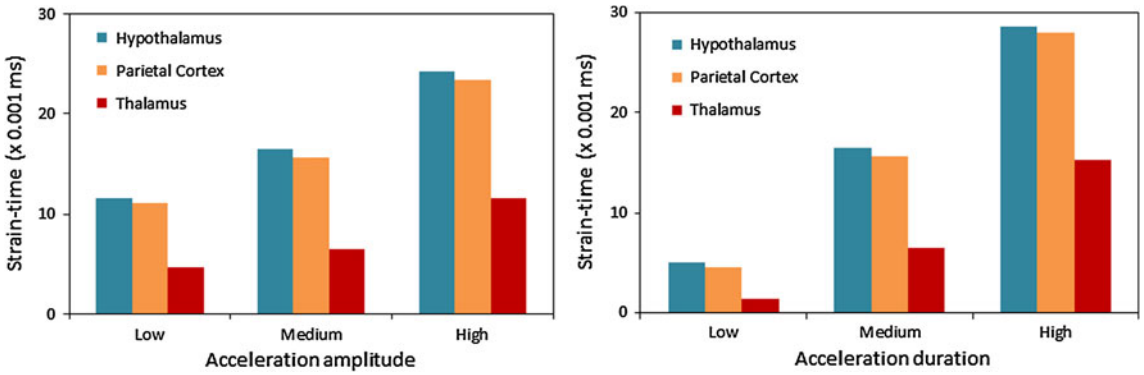

Fig. 11 Bar chart showing strain-time responses in the different regions of the brain. *Left* shows variations with increasing magnitude of applied rotational acceleration (fixed duration), and *right* shows variations with increasing magnitude of duration (fixed acceleration). Note similar trends in both groups (*left* and *right*)

Table 4 Results of linear regression analysis correlating unconscious time with stress and strain data

Parameter	Details	Anatomical region		
		Hypothalamus	Parietal cortex	Thalamus
Strain	Slope [10^3 s]	9.732	9.926	15.626
	R^2	0.4134	0.4076	0.3734
Stress	Slope [s.Pa^{-1}]	0.301	0.308	0.459
	R^2	0.4128	0.4064	0.3761
Strain-time	Slope [10^6]	15.210	15.724	31.618
	R^2	0.9120	0.9196	0.9499
Stress-time	Slope [10^3 Pa^{-1}]	0.461	0.471	0.800
	R^2	0.9202	0.9277	0.9450

controlled experimental setup. The used regional components are pertinent to mild TBI. We are not aware of any similar studies on the human, and recognizing fundamental differences in the brains between the current animal model and the human, such as compositions of gray and white matters, the present study should be considered as a first step in an improved understanding of the intrinsic biomechanics of mild TBIs induced by angular loading. Furthermore, it should be noted that the experimental animal model used in the present study has long been used by brain injury researchers including biomechanical engineers, finite element modelers and basic scientists. Also, while rat and human brains have many noticeable differences (in size, shape, white matter distribution, gyri, etc.), at the tissue or cellular level they are more comparable [39]. So, information on lesions and thresholds from the rat model is not irrelevant for injury mechanisms. Consequently, additional studies are needed to fully understand the mechanics of mild TBIs in the human.

4.2 Rationale for selecting the three anatomical regions

Biomechanical variables examined in the present study at three anatomical locations, i.e., the hypothalamus, thalamus and parietal cortex, were correlated with the times of loss of consciousness from animals exposed to differing levels of rotational acceleration and duration. The rationale is as follows for the selection of the three regions [18, 43]. While precise mechanisms for the loss of consciousness are yet to be substantiated, several anatomical entities are considered by basic neuroscience, clinical and other

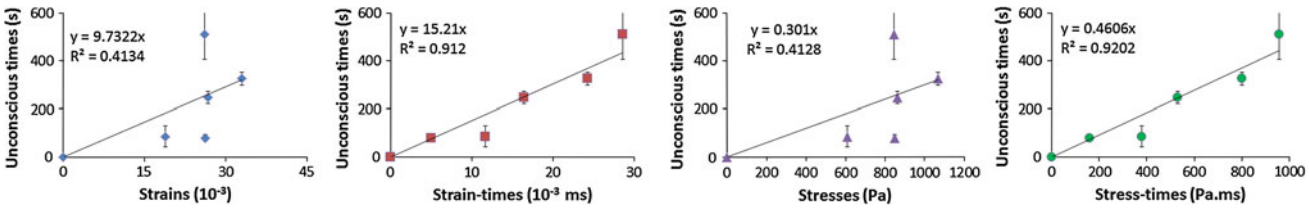

Fig. 12 Data points in the hypothalamus and their associated linear regression trends

investigators. In the human, different components/regions of the brain account for specific functions, although no single component acts in isolation, i.e., interconnectivity exists. Focusing on consciousness, the activation of the neurophysiological systems occurs to this sensation. Subcortical scanning leads to the involvement of the thalamus, which in turn projects into the prefrontal association cortex consisting of the posterior inferior temporal and parietal and bilateral association cortices. The maintenance or loss of consciousness depends on the interaction between the brainstem, thalamus, hypothalamus and cortical activity. The reticular activating system of the brainstem must be intact for the conscious state, and the hypothalamus and cerebral cortex provide signals to this system. The cell bodies of the activating system are located in the thalamus. It was thus decided to examine intrinsic responses of the hypothalamus, thalamus and parietal cortex to achieve the objectives of the present study. Structural damage to these regions stemming from mechanical insults such as those used in the current model, individually or collectively, may contribute to the primary effects of consciousness or its lack thereof. It should be noted that the three areas of brain analyzed are correlations, not causations, of unconsciousness. It should also be added that the brainstem responses were observed in the model. But, while the brainstem has a role in the mechanisms of consciousness, it did not display any significant stresses or strains in the simulation. This is certainly linked to the fact that the mesh limits itself to the brain, diminishing the boundary conditions that a complete spinal cord would impose on the brainstem.

The selection of the three regions is further supported by physical and primate experiments conducted in 1943 and 1974 [17, 35]. Using the centripetal theory as a basis, and applying rotational accelerations to primates, a mode similar to the present study, clinical concussion was attributed to stresses/strains initiating from the surface (cortex, mild cases) and progressing towards the diencephalic and mesencephalic cores (more severe cases). The extractions of stresses/strains in the thalamus components located in the former core along with the peripheral cortex are appropriate. Furthermore, while peak magnitudes have been proposed as a metric to characterize brain injuries, especially DAI, recent studies have shown that trauma is region dependent and pulse-shape dependent [11, 45]. In fact, this was an impetus to examine the stress analysis outputs in the three anatomical regions and in two groups of insults, acceleration and duration. The region dependency was based on the loss of consciousness, as discussed above, and the stress analysis outputs were examined for different parameters, as discussed below.

4.3 Rationale for evaluating stress variables

As indicated in the Introduction, although finite element models of the rat brain were developed to simulate DCDs [38] to study injuries to the blood–brain barrier; controlled cortical impacts [28, 36] and closed head injuries [22] to complement experimental indentation data [12]; and inertial loading to examine strain-time-based parameters for hippocampal damage [11], the present model is the first complete three-dimensional mild TBI-specific model to correlate stress- and strain-related data at the hypothalamus, parietal cortex and thalamus with loss of consciousness. Because previous studies correlated the peak Von Mises stress with neurological outcomes in animal and human models, this variable was included in the present study [2–4, 41]. This metric may also be used as a candidate for mild TBI, as stresses in all regions increased with increasing unconscious times, associated with increasing peak accelerations. However, the metric did not follow the same pattern with increasing pulse times, reflecting its limited application. It was for this reason the stress-time metric was examined for its potential effectiveness. As indicated in the previous section, this metric was found to be a better correlate than the pure peak stress parameter in these mild TBI cases. Although not fully established, the present analysis may have discovered a new metric to characterize mild TBI.

As for the significance of such integrated new metrics, a comparison can be established with a variable consisting of deformation and time that had been used in earlier research [11]. Sustained maximum principal strain had been used as a metric in a slice model of the brain. The present study follows a similar pattern although the difference is that we used integrated strain-time (and stress-time) as a metric in the three-dimensional model in contrast to a preselected strain level over a preselected time. An implied physical meaning is that the mechanics of the brain tissue may be

characterized by cumulative strain, determined by the integral of the variable with time, and including the notion of mechanical wear and tear of brain matter.

4.4 Comparison with literature

A comparison of results from the present study with the literature indicates the following. Finite element modeling studies have reported greater magnitudes of strains than those found in the present study. In 2006, based on controlled cortical impact loading applied to a rat finite element model, Mao et al. [28] reported that a strain level of 0.30 represents contusive brain injury. Kleiven et al. [21] used the maximum principal strain as a metric for predicting concussion: 50 % risk of concussion was estimated at a strain level of 0.21 in the corpus callosum and the same magnitude was also applicable for the gray matter. In 2008, using the Strasbourg University Finite Element Head Model, the first principal strain was proposed as a criterion to assess DAI: a strain level of 0.31 corresponded to 50 % injury risk [6]. However, Sabet et al. [37] observed deformations in the human volunteers under mild angular acceleration loading using tagged magnetic resonance images and reported that large portions of the brain sustain strains exceeding 0.02. Most of the aforementioned studies dealt with conditions different from the present study: some had direct contact impact, creating high strains near the contact interface [28]; and other studies were based on experimental or numerical models of the human brain [6, 37]. Differences in the strain level may be due to these variations.

In the current three-dimensional model, the rat head was subjected to inertial loadings without direct contact. This necessitated the application for greater levels of loadings/rotational acceleration to achieve outcomes similar to those observed in the human [17, 31, 34]. It also has consequences on the direct response of the finite element modeling of the brain. Using a human brain finite element model, it has been shown that the size of the brain model affects the biomechanical outputs such as internal stresses [20]. It has also been observed that a smaller-sized brain model would result in lower deformations overall, in a study comparing adult and child human brain models [29]. Consequently, while strains from the current model could be seen as a little low, there is a possibility that these values are linked to the small size of a rat brain. And though strains appear a bit low, strain rates as shown in Fig. 6 were of the same order of magnitude reported in an earlier study [19]. In the cited study, 25 % risk of injury was associated with a strain rate of 46 per second, and this was based on logistic regression analysis, as defined by the −2 log likelihood ratio score and Wald Chi Squared statistics. Furthermore, it should be noted that external loadings used in the present simulations were aimed to produce only mild TBI, and among the aforementioned works, only the work of Sabet et al. aimed at mild TBI. Indeed, the strains in the current work are in the magnitude order of the 0.02 strains reported by Sabet et al. acknowledging the above discussion, the present study has relevance to the application of mild TBI.

To confirm the estimated strain levels, as a first step, the current three-dimensional rat finite element model was exercised at rotational accelerations similar to a study conducted in 2009 for the analysis of DAI under rearward accelerations [5]. In the 2009 study, a 1.5 Mrad/s^2 acceleration pulse of 0.5 ms duration resulted experimentally in damaged axons in the hippocampus region, while the model predicted its highest stresses in the corresponding anatomical component. In the current study, the hypothalamus responded with a peak strain of approximately 15 % for this DAI loading case, a magnitude considerably greater than peak strains found in the current mild TBI model. Hence, it appears that strain data from the present study are in-line with the pulse severity, although correlations of the predicted magnitudes from this model with the human brain remain to be explored.

Also of interest are the relative magnitudes of strains and stresses in the three studied anatomical regions of the brain. The highest values were reported in the hypothalamus, then in the parietal cortex, and would be the lowest in the thalamus. This would be in accordance with the centripetal force theory [35], as in our model the hypothalamus is situated along the lower surface of the brain while the thalamus is one of the most central parts and closer to the centre of rotation. At the same time, this observation also points towards some perspectives for the FE model. It is considered homogeneous and made only of gray matter. However, a differentiation between gray and white matter properties could affect the results of the model. To achieve this, a refinement of the mesh may be needed. Such extensions considerably increase computational times. Associated with the already depicted sub-components of the cerebrum, it could allow having an anatomically related definition of material properties. These are considered as future research directions.

5 Conclusion

Anatomical region-dependent mechanical responses of the brain in mild TBI cases were investigated through a combined approach of animal experiments of head coronal plane angular accelerations and a finite element model of the rat brain and skull. These responses, stresses and strains, were obtained through the computational model and were correlated to the behavioral evidence of injury in rats submitted to the same experimental setup, i.e., loss of

consciousness times. The acceleration pulses, both in experiments and simulations, were designed to obtain independent gradations of amplitude and duration. While the strains and Von Mises stresses matched variations of peak angular acceleration in the hypothalamus, parietal cortex and thalamus, similar trends were not obvious for variations in the duration of the rotational acceleration. Consequently, two time-integrated metrics were explored. They proved to be better suited for the prediction of the variations in injury severity associated with both the amplitude and duration of the loading pulses. These metrics, strain-time and stress-time, were well correlated with experimentally observed loss of consciousness times. Results of our hybrid approach indicate that new time-integrated metrics may be better suited to explain the mechanics of mild TBI.

References

1. AIS (1990) The abbreviated injury scale. American Association for Automotive Medicine, Arlington Heights, IL, p 74
2. Anderson RW, Brown CJ, Blumbergs PC, Scott G, Finnie J, Jones NR, McLean AJ (1999) Mechanisms of axonal injury: an experimental and numerical study of a sheep model of head impact. In: Proceedings of the IRCOBI Conference, pp. 107–120
3. Anderson RW, Brown CJ, Blumbergs PC, McLean AJ, Jones NR (2003) Impact mechanics and axonal injury in a sheep model. J Neurotrauma 20(10):961–974
4. Baumgartner D, Willinger R (2004) Human head tolerance limits to specific injury mechanisms inferred from real world accident numerical reconstruction. Revue Europeenne des Elements Finis 14(4–5):421–444
5. Davidsson J, Risling M, Angeria M (2009)A new model and injury threshold for sagittal plane rotational induced diffuse axonal injuries in the brain. IRCOBI York, England, pp 73–80
6. Deck C, Willinger R (2008) Improved head injury criteria based on head FE model. Int J Crashworthiness 13(6):667–678
7. Dixon CE, Lyeth BG, Povlishock JT, Findling RL, Hamm RJ, Marmarou A, Young HF, Hayes RL (1987) A fluid percussion model of experimental brain injury in the rat. J Neurosurg 67(1):110–119
8. Dixon CE, Clifton GL, Lighthall JW, Yaghmai AA, Hayes RL (1991) A controlled cortical impact model of traumatic brain injury in the rat. J Neurosci Methods 39(3):253–262
9. Faul M, Xu L, Wald M, Coronado V (2010) Traumatic brain injury in the United States: Emergency Department Visits, Hospitalizations and Deaths, Centers for Disease Control and Prevention, National Center for Injury Prevention and Control, Atlanta, GA
10. Fijalkowski RJ, Stemper BD, Pintar FA, Yoganandan N, Crowe MJ, Gennarelli TA (2007) New rat model for diffuse brain injury using coronal plane angular acceleration. J Neurotrauma 24(8): 1387–1398
11. Fijalkowski RJ, Yoganandan N, Zhang J, Pintar FA (2009) A finite element model of region-specific response for mild diffuse brain injury. Stapp Car Crash J 53:193–213
12. Gefen A, Gefen N, Zhu Q, Raghupathi R, Margulies SS (2003) Age-dependent changes in material properties of the brain and braincase of the rat. J Neurotrauma 20(11):1163–1177
13. Gennarelli TA, Thibault LE, Adams JH, Graham DI, Thompson CJ, Marcincin RP (1982) Diffuse axonal injury and traumatic coma in the primate. Ann Neurol 12(6):564–574
14. Gennarelli TA, Meaney DF (1996) In: Wilkins NR, Rengachary S (eds) Mechanisms of primary head injury. McGraw Hill, New York, pp 2611–2621
15. Greenberg M (2010) Handbook of Neurosurgery. Thieme, New York, NY
16. Guan F, Han X, Mao H, Wagner C, Yeni YN, Yang KH (2011) Application of optimization methodology and specimen-specific finite elements models for investigating material properties of rat skull. Ann Biomed Eng 39(1):85–95
17. Holbourn AHS (1945) The mechanics of brain injuries. Br Med Bull 3:144–149
18. Kandel E, Schwartz J, Jessell T (2000) Principles of neural science. McGraw-Hill, New York, NY
19. King A, Yang KH, Zhang L, Hardy WN (2003) Is head injury caused by linear or angular acceleration?. IRCOBI Lisbon, Portugal, pp 1–12
20. Kleiven S, von Holst H (2002) Consequences of head size following trauma to the human head. J Biomech 35(2):153–160
21. Kleiven S (2007) Predictors for traumatic brain injuries evaluated through accident reconstructions. Stapp Car Crash J 51:81–114
22. Levchakov A, Linder-Ganz E, Raghupathi R, Margulies SS, Gefen A (2006) Computational studies of strain exposures in neonate and mature rat brains during closed head impact. J Neurotrauma 23(10):1570–1580
23. Lighthall JW (1988) Controlled cortical impact: a new experimental brain injury model. J Neurotrauma 5(1):1–15
24. Lindgren S, Rinder L (1969) Production and distribution of intracranial and intraspinal pressure changes at sudden extradural fluid volume input in rabbits. Acta Physiol Scand 76(3):340–351
25. Lissner HR, Lebow M, Evans FG (1960) Experimental studies on the relation between acceleration and intracranial pressure changes in man. Surg Gynecol Obstet 111:329–338
26. Luethcke CA, Bryan CJ, Morrow CE, Isler WC (2010) Comparison of concussive symptoms, cognitive performance, and psychological symptoms between acute blast-versus nonblast-induced mild traumatic brain injury. J Int Neuropsychol Soc 17(1):36–45
27. Macgregor AJ, Dougherty AL, Galarneau MR (2010) Injury-specific correlates of combat-related traumatic brain injury in operation iraqi freedom. J Head Trauma Rehabil 26(4):312–318
28. Mao H, Zhang L, Yang KH, King AI (2006) Application of a finite element model of the brain to study traumatic brain injury mechanisms in the rat. Stapp Car Crash J 50:583–600
29. Mao H, Gao H, Cao L, Genthikatti VV, Yang KH (2011) Development of high-quality hexahedral human brain meshes using feature-based multi-block approach. Comput Methods Biomech Biomed Eng 1–9. doi:10.1080/10255842.2011.617005
30. Mao H, Wagner C (2011) Material properties of adult rat skull. J Mech Med Biol 11(5):1199–1212
31. Margulies SS, Gennarelli T (1985) A study of scaling and head injury criteria using physical model experiments. International research council on the biomechanics of impact (IRCOBI) sitges. Spain
32. Marion DW, Curley KC, Schwab K, Hicks RR, The Mtbi Diagnostics Workgroup (2010) Proceedings of the military mTBI diagnostics workshop held in St. Pete Beach, August 2010. J Neurotrauma 28(4):517–526
33. Marmarou A, Foda MA, van den Brink W, Campbell J, Kita H, Demetriadou K (1994) A new model of diffuse brain injury in rats. Part I: pathophysiology and biomechanics. J Neurosurg 80(2):291–300
34. Ommaya AK, Yarnell P, Hirsch AE (1967) Scaling of experimental data on cerebral concussion in subhuman primates to

concussion threshold for man. 11th Stapp car crash conference, pp 73–80
35. Ommaya AK, Gennarelli TA (1974) Cerebral concussion and traumatic unconsciousness. Correlation of experimental and clinical observations of blunt head injuries. Brain 97(4):633–654
36. Pena A, Pickard JD, Stiller D, Harris NG, Schuhmann MU (2005) Brain tissue biomechanics in cortical contusion injury: a finite element analysis. Acta Neurochir Suppl 95:333–336
37. Sabet AA, Christoforou E, Zatlin B, Genin GM, Bayly PV (2008) Deformation of the human brain induced by mild angular head acceleration. J Biomech 41(2):307–315
38. Shreiber DI, Bain AC, Meaney DF (1997) In vivo thresholds for mechanical injury to the blood-brain barrier. 41st Stapp car crash conference, pp 277–292
39. Shreiber DI, Bain AC, Ross DT, Smith DH, Gennarelli TA, McIntosh TK, Meaney DF (1999) Experimental investigation of cerebral contusion: histopathological and immunohistochemical evaluation of dynamic cortical deformation. J Neuropathol Exp Neurol 58(2):153–164
40. Shuck LZ, Advani SH (1972) Rheological response of human brain tissue in shear. J Basic Eng 94:905–911
41. Tagliaferri F, Compagnone C, Korsic M, Servadei F, Kraus J (2006) A systematic review of brain injury epidemiology in Europe. Acta Neurochir (Wein) 148:255–268
42. Vappou J, Breton E, Choquet P, Willinger R, Constantinesco A (2008) Assessment of in vivo and post-mortem mechanical behavior of brain tissue using magnetic resonance elastography. J Biomech 41:2954–2959
43. Winn R (2004) Neurological surgery. Saunders, Philadelphia, PA
44. Yoganandan N, Pintar FA, Larson SJ, Sances A Jr (eds) (1998) Frontiers in head and neck trauma: clinical and biomechanical. IOS Press, The Netherlands
45. Yoganandan N, Li J, Zhang J, Pintar FA, Gennarelli TA (2008) Influence of angular acceleration-deceleration pulse shapes on regional brain strains. J Biomech 41(10):2253–2262
46. Zhang J, Yoganandan N, Pintar FA, Gennarelli TA (2006) Brain strains in vehicle impact tests. Annu Proc Assoc Adv Automot Med 50:1–12
47. Zhu F, Mao H, Lineonardi A, Wagner C, Chou C, Jin Z, Bir C, Vandervord P, Yang KH (2010) Development of a finite element model of the rat head subjected to air shock loading. Stapp Car Crash J 54:211–225